A Novel CuII/8-Aminoquinoline Isomer Complex [Cu(H2O)2(C9H8N2)2]Cl2: Solvothermal Synthesis, Molecular Structure, Hirshfeld Surface Analysis, and Computational Study

Zouaoui Setifi, Hela Ferjani, Youssef Ben Smida, Christian Jelsch, Fatima Setifi, Christopher Glidewell

Published in Chemistry Africa. 2022, 1-11. https://doi.org/10.1007/s42250-022-00523-0

A Novel Cu^{II}/8-Aminoquinoline Isomer Complex $[Cu(H_2O)_2(C_9H_8N_2)_2]Cl_2$: Solvothermal Synthesis, Molecular Structure, Hirshfeld Surface Analysis, and Computational Study

Zouaoui Setifi[1,2], Hela Ferjani[3,*], Youssef Ben Smida[4], Christian Jelsch[5], Fatima Setifi[1,*], Christopher Glidewell[6]

[1]Laboratoire de Chimie, Ingénierie Moléculaire et Nanostructures (LCIMN), Université Ferhat Abbas Sétif 1, Sétif 19000, Algeria
[2]Département de Technologie, Faculté de Technologie, Université 20 Août 1955-Skikda, Skikda 21000, Algeria
[3]Chemistry Department, College of Science, IMSIU (Imam Mohammad Ibn Saud Islamic University), Riyadh 11623, Kingdom of Saudi Arabia
[4]Laboratory of Valorization of Useful Materials, National Center of Materials Sciences Research, Techno Park Borj Cedria, Carthage University, Soliman, Tunisia.
[5]CRM2 , CNRS, Institut Jean Barriol, Université de Lorraine, 54000, Nancy, France
[6]School of Chemistry, University of St Andrews, St Andrews, Fife, KY16 9ST, UK
Corresponding authors: hhferjani@imamu.edu.sa (Hela Ferjani); fat_setifi@yahoo.fr (Fatima Setifi)

Zouaoui Setifi: (ORCID: https://orcid.org/0000-0002-8160-3852)
Fatima Setifi: (ORCID: https://orcid.org/0000-0002-9860-9310)
Hela Ferjani: (ORCID: https://orcid.org/0000-0001-8048-847X)
Youssef Ben Smida: (ORCID: https://orcid.org/0000-0001-7820-0318)

ABSTRACT

A new isomer $[Cu(H_2O)_2(C_9H_8N_2)_2]Cl_2$ complex **(1)**, has been synthesized by solvothermal method. The single-crystal X-ray study, Hirshfeld surface analysis and computational calculation were discussed. The hydrogen bonding network within the complex enables the formation of a 3D network supported by the aromatic stacking interactions of quinoline rings in face-to-face and edge-to-face fashions. The analysis of Hirshfeld surfaces facilitates a comprehension of intermolecular interactions in the structure. The reactivity descriptors for **(1)** such as E_{HOMO} and E_{LUMO} energies, density of state (DOS), ionization potential (IP), electron affinity (EA), Mulliken electronegativity (χ) and the absolute hardness (η) were calculated by the PBE functional method with the DNP basis set. The possible sites for nucleophilic and electrophilic attacks on **(1)** were analyzed through Fukui functions.

Keywords: Crystal structure; Copper (II) complex; Non-Covalent Interactions; Hirshfeld surface analysis; Reactivity descriptors; Fukui functions.

1. Introduction

One of the most rapidly developing fields of modern inorganic chemistry is the synthesis and study of metal complexes based on heterocyclic ligands. The breadth of their potential practical applications drives ongoing research in this area. Ligands containing N, X-donor (X = O, S) heterocyclic chelators are very important compounds [1-10] that have provided tremendous opportunities for the discovery of enormous novel coordination species with significant potential applications in medicine [11], magnetism [12], catalysis [13], and luminescence [14]. 8-Aminoquinoline and its derivatives are systems that have been recently undertaken because of their antiprotozoal activities and other medicinal properties [14-16]. They have also been used to prepare new adjustable molecular materials [17-19]. Different functionalized molecules of 8-aminoquinoline have been described [20-22]. However, the coordination chemistry of 8-aminoquinoline, as such, is less cited in the literature [23, 24].

Transition metals and polynitrile ligands such as dicyanamide, dca (dca = $N(CN)_2^-$) have been used to create coordination polymers [25-28]. The flexible coordination and bridging modes of dca include $\mu_{1,3}$ (coordinating through one nitrile nitrogen atom and the other nitrogen atom), $\mu_{1,5}$ (coordinating through the two nitrile nitrogen atoms) and $\mu_{1,3,5}$ (coordinating through all three nitrogen atoms). Furthermore, the ligand's negative charge indicates that additional anions are not required to balance the charge in the structures formed [29, 30]. The addition of co-ligands during synthesis can change the structure type and network of coordination polymers. Given the dicyanamide ligand's important role, we became interested in combining it with other chelating or bridging neutral co-ligands to create and produce new coordination polymeric materials. As a continuation of our efforts to design such polymeric compounds with diverse structures and magnetic properties [31-34], the title complex was unexpectedly obtained. So, we decided to study the influence of the metal ion and his counter-ion on crystalline networks and also the importance of the hydrogen-bonding and the π-stacking interactions in the crystal. The role of these interactions in crystal engineering is currently of great interest due to their use in constructing two- and three-dimensional polymers. We herein report the synthesis and detailed studies of a novel copper (II) complex bearing an aqin ligand (aqin=8-aminoquinoline) by single crystal X-ray crystallography and computational methods.

2. Experimental

2.1. Materials and Synthesis

All chemicals were furnished from commercial sources and used without further purification. A PerkinElmer 2400 series II CHNS/O analyzer was used for element analysis (C, H, and N). The solid-state absorption IR spectrum was recorded in the 4000-500 cm^{-1} frequency range using a Nicolet 5SX-FTIR spectrometer installed with a diamond micro-ATR accessory.

Complex **(1)** was prepared by solvothermal synthesis under autogenous pressure. A mixture of copper (II) chloride dihydrate (17 mg, 0.1 mmol), 8-aminoquinoline (29 mg; 0.2 mmol) and sodium dicyanamide (18 mg, 0.2 mmol) in H_2O/MeOH (3:1 v/v, 20 mL) was agitated for 30 min and moved to a Teflon-lined autoclave. The autoclave is then heated at 180 °C for 3 days. After slowly cooling at a rate of 10 °C/h at room temperature, light violet crystals of **(1)** were obtained, and are suitable for X-ray diffraction study. Anal. Calcd. (%) for $C_{18}H_{20}Cl_2CuN_4O_2$: C, 47.12; H, 4.39; N, 12.23%. Found: C, 46.87; H, 4.48; N, 12.54%. IR (ATR, cm^{-1}): 3365 (O-H); 3228, 3151 (N-H); 1503, 1477 (C=C); 1379 (C=N); 889 (C-N). mp 215 °C.

2.2. X-ray crystallography

The X-ray diffraction data were collected at 100 K using an Agilent Xcalibur Sapphire1 diffractometer, equipped with a graphite-monochromatised Mo *K*α radiation (λ= 0.71073 Å). A multi-scan [35] absorption correction was applied. The structure was solved and refined by full-matrix least squares based on F^2 using SHELXS-97 and SHELXL-97 [36], respectively. The hydrogen atoms were treated as riding atoms and refined with N-H, O-H and C-H distances fixed at 0.89, 0.83 and 0.95 Å, respectively, with U_{iso} (H) values of $1.2U_{eq}$ (N, O and C). The molecular graphics were prepared using *Diamond 3* program [37].

Crystal data and data collection procedures are summarized in Table 1. Crystallographic structural data has been deposited at the Cambridge Crystallographic Data Centre (CCDC). Enquiries for data can be directed to: Cambridge Crystallographic Data Centre, 12 Union Road, Cambridge, UK, CB2 1EZ or (e-mail) deposit@ccdc.cam.ac.uk or (fax) +44 (0) 1223 336033. Any request to the Cambridge Crystallographic Data Centre for this material should quote the full literature citation and the reference number CCDC 2054557.

Table 1. Crystal data and structure refinement parameters for **(1).**

Empirical formula	**$[Cu(H_2O)_2(C_9H_8N_2)_2].2Cl$**
Chemical name	Diaqua-bis(8-quinolinamine)-copper(II) dichloride
Formula weight (g/mol)	458.82
Crystal system, space group	Monoclinic, *P2₁/n*
***a* (Å)**	8.3834 (7)
***b* (Å)**	7.8236 (6)
***β* (°)**	102.594 (8)°
***V* (Å^3)**	942.60 (13)
***μ* (mm^{-1})**	1.46
D_x (Kg m^{-3})	1.617 10^{-6}
***F*(000)**	470
Crystal size (mm)	0.35 × 0.30 × 0.05
Crystal habit	Plate, light purple
θ_{min} / θ_{max} (deg)	3.9/27.6°
Measured reflections	5574
Independent reflections	2164
Observed refl. with I> 2σ(I)	1843
R_{int}	0.039
Data/restraints/parameters	2164 /4/136
***R*[F^2> 2σ(F^2)]**	0.038
***wR*(F^2)**	0.086
GooF=*S*	1.06
$\Delta\rho_{max}$ / $\Delta\rho_{min}$ (e.Å^{-3})	0.44 /-0.42
CCDC Number	2 054 557

3. Theoretical methods

3.1. Hirshfeld surface calculations

The contact proportions on the Hirshfeld surface and their enrichment were computed with the MoProViewer software [38]. The contact enrichment ratio E_{xy} between chemical species X and Y is obtained by comparing the actual contacts C_{xy} in the crystal with those computed as if all types of contacts were equiprobable. The nature of contacts and their enrichment in the crystal packing are shown in Table 5. To obtain an integral Hirshfeld surface around each moiety (Cu(II) cation, chloride anion and organic ligand), a set of entities not in contact with each other were selected in the crystal packing.

3.2. Computational details

The Frontier Molecular Orbitals HOMO (Highest Occupied Molecular Orbital energy) and LUMO (Lowest Unoccupied Molecular Orbital energy), density of states (DOS), and the Fukui indices of the asymmetric unit of **(1)** have been obtained by using the DMol3 code [39]. The calculations were carried out by means of Mulliken and Hishfeld population analysis [40] and by using the PBE functional method with DNP basis set [41]. The convergence parameters were as follows: maximum displacement of 0.005 Å, SCF tolerance 1×10^{-6} eV/atom and convergence energy tolerance 1×10^{-6} Ha.

4. Results and Discussion

4.1. Crystal structure description

X-ray crystal structure analysis reveals that **(1)** crystallizes in the monoclinic space group $P2_1/n$. The asymmetric unit comprises one half of the complex cation $[Cu(H_2O)_2(C_9H_8N_2)_2]^{2+}$ and one chloride counter-anion (Figure 1). The Cu^{II} atom lies on an inversion center (Figure 2). In the cation complex, the Cu^{II} atom is coordinated in a slightly distorted octahedral manner by four N atoms from two chelating 8-aminoquinoline ligands and two axially coordinated water molecules. The N1-Cu-$N1^i$ and N2-Cu-$N2^i$ angles [symmetry code: (i) -x+1, -y+1, -z+1] are linear (180°). The *cis* bond angles around the Cu^{II} atom range from 83.44 (8)-96.56 (8) Å. The Cu-N bond lengths range from 2.007 (2) to 2.023 (2) Å (Table 2). These bond lengths are like those observed in similar structures containing 8-aminoquinoline ligands [42-44]. The axial Cu-OW1 bond (2.431(17) Å) is remarkably longer than the equatorial Cu-N distances (Table 2) because of the Jahn-Teller effect [45]. The 8-aminoquinoline ligands exhibit a *planar* coordination mode in which the angle between the planes defined by the Cu/N1/C9/C8/N2 and

N2/C8/C9/N1 of the 8-aminoquinoline ligand is 7.37 (7)º (Figure 3). The chelating ring formed by the chelation of ligand to the central metal atom (Cu1/N1/C9/C8/N2) is close to planar with an r.m.s deviation of 0.069.

Non-covalent interactions such as hydrogen-bonding interactions and aromatic stacking interactions provide extreme stability to the structure. Chloride anions are linked to the cationic complex through two sets of strong hydrogen bonds: two N2-H21/22···Cl1$^{ii/iii}$ {(ii)= -x+$^3/_2$, y-½, -z+$^3/_2$; (iii) = x-½, -y+½, z-½} with the amino protons of the NH2-quinoline ligand and two O1W-H11/12···Cl1/Cl1^{ii} with the coordinated water molecules, forming a two-dimensional hydrogen-bonding network (Figure 4a, Table 3). The cationic complexes situated around z=½ are connected through face-to-face stacking interaction between the quinoline rings {Cg3-Cg3^i = 3.521 (3), Cg3-Cg4^i = 3.839 (4) Å where Cg3 is the centroid of the ring N1-C9, Cg4 is the centroid of the ring C4-C9; i: symmetry code: -x,1-y,1-z } (Figure 4b) and by edge-to-face stacking interaction between the quinoline rings placed at z=0 and z=½ {Cg4-Cg3^i = 4.431 (3), i: symmetry code: -x,1-y,1-z } (Figure 4c). The facility to undergo hydrogen bonds and stacking interactions is a suitable tool in the formation of a self-assembled structure.

The structure of **(1)** represents another isomer of a previously reported structure of $[Cu(C_9H_8N_2)_2(Cl)(H_2O)]^+.(Cl^-).H_2O$ [46] **(2)** (Figure 5). The single crystal X-ray diffraction analysis of isomers **(1)** and **(2)** reveals that their space groups, unit cell parameters, and Z values follow a different symmetry order. When comparing the structural parameters of isomers **(1)** and **(2)**, the similarity in the two complexes is reflected in the coordinative copper (II) center with two bidentate chelating 8-aminoquinoline. And the difference between the two structures is related to their occupancy of vertices axes. However, the chloride anion and water molecules in the isomer **(2)** assume the roles of the counter anion and coordinative ligands, respectively. The Cu-N (1.985 (9)-2.033 (10) Å) and Cu-O (2.566(6)Å) bond lengths are within normal ranges, with one exception controlled by the Cl coordinative atom **(Table 4)** [47]**.** The crystal packing of isomer **(2)** is stabilized by different N-H···Cl and O-H···Cl hydrogen bonding interactions. When the coordinated halogen atom Cl interacts with the metal cation and a neighboring NH_2 group at the same time, a supplementary N-H···Cl hydrogen bond is formed. The linearity of the vertex's axes (Cl1-Cu1-O2=172.51°) is affected by this type of hydrogen bond, which was not the case for the isomer **(1)** (OW1-Cu1-OW1= 180°). Furthermore, a supplementary N-H···O hydrogen bond exists between the quinoline rings and the uncoordinated water molecule.

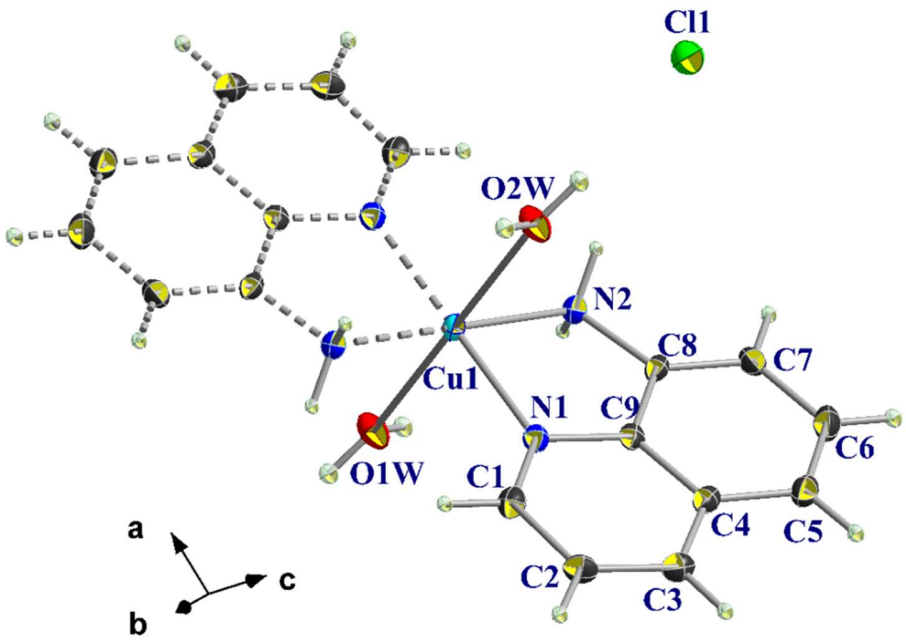

Fig. 1. A view of the molecular structure of **(1)**, with atom labelling. Displacement ellipsoids are drawn at the 50% probability level. Unlabeled atoms (dashed bonds) are related to the labelled atoms by inversion symmetry (Symmetry operation: 1-x, 1-y, 1-z).

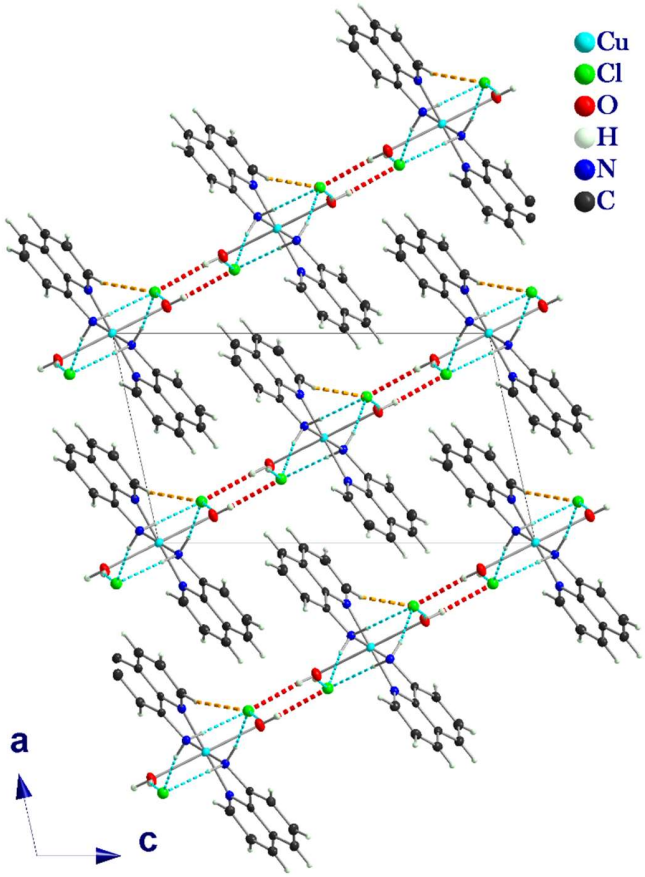

Fig. 2. A view of the crystal packing of **(1)**, showing the alternating cationic complex chains and chlorine anions connected through hydrogen bonds.

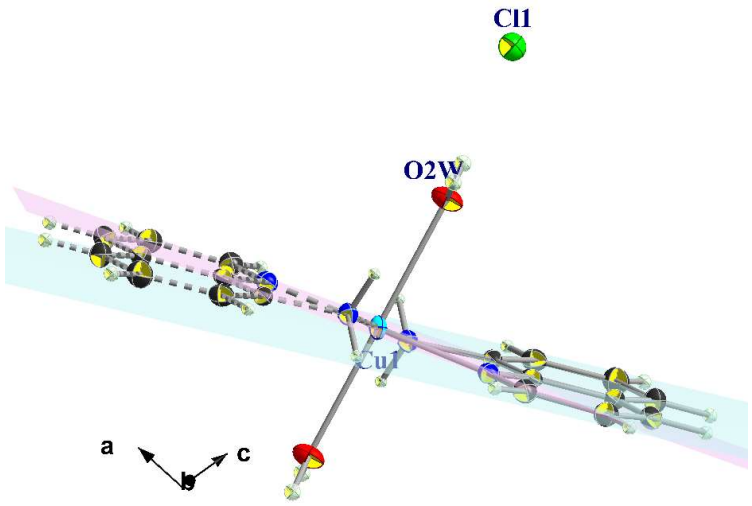

Fig.3. A planar coordination mode of 8-aminoquinoline ligand (Angles between pink and blue planes =7.37 (7)°).

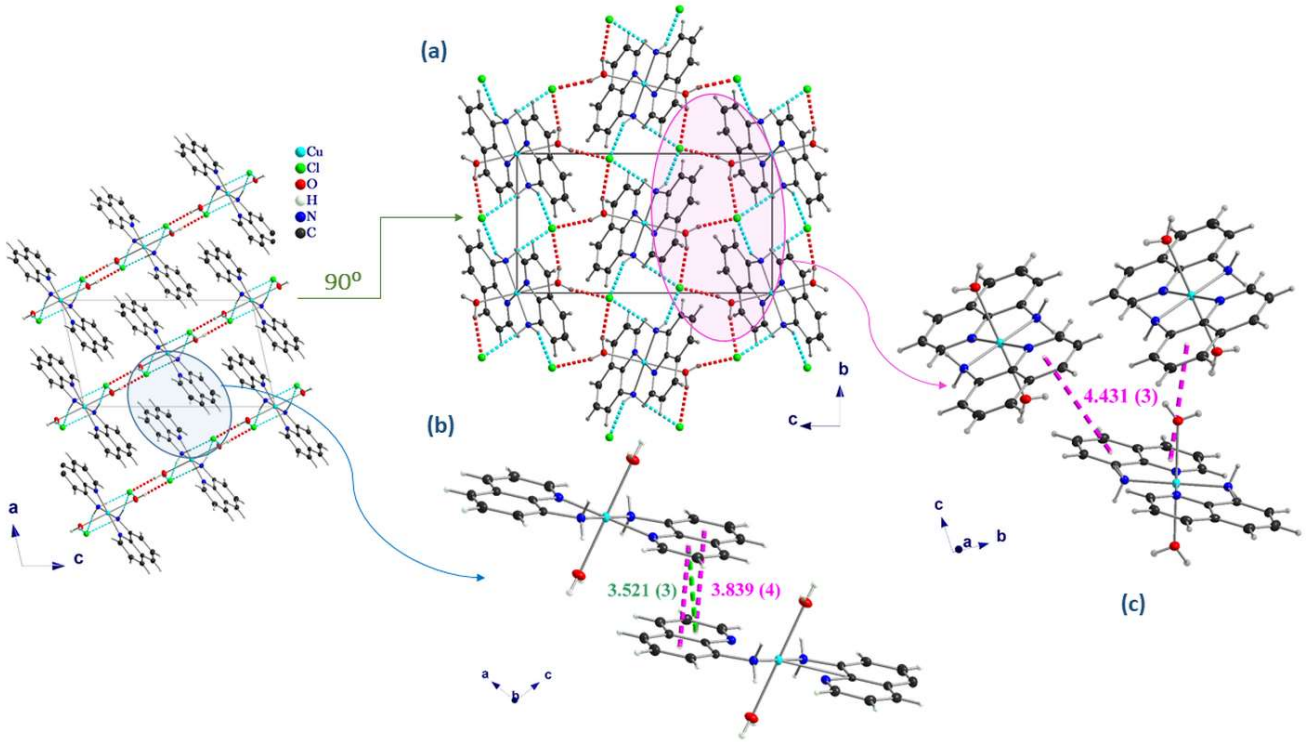

Fig. 4. (a) View along *a* axis of the packing diagram showing hydrogen- bonding interactions (cyan and red dashed lines) **(b)** Face-to-Face stacking interactions and **(c)** Edge-to-Face stacking interaction (green and pink dashed lines).

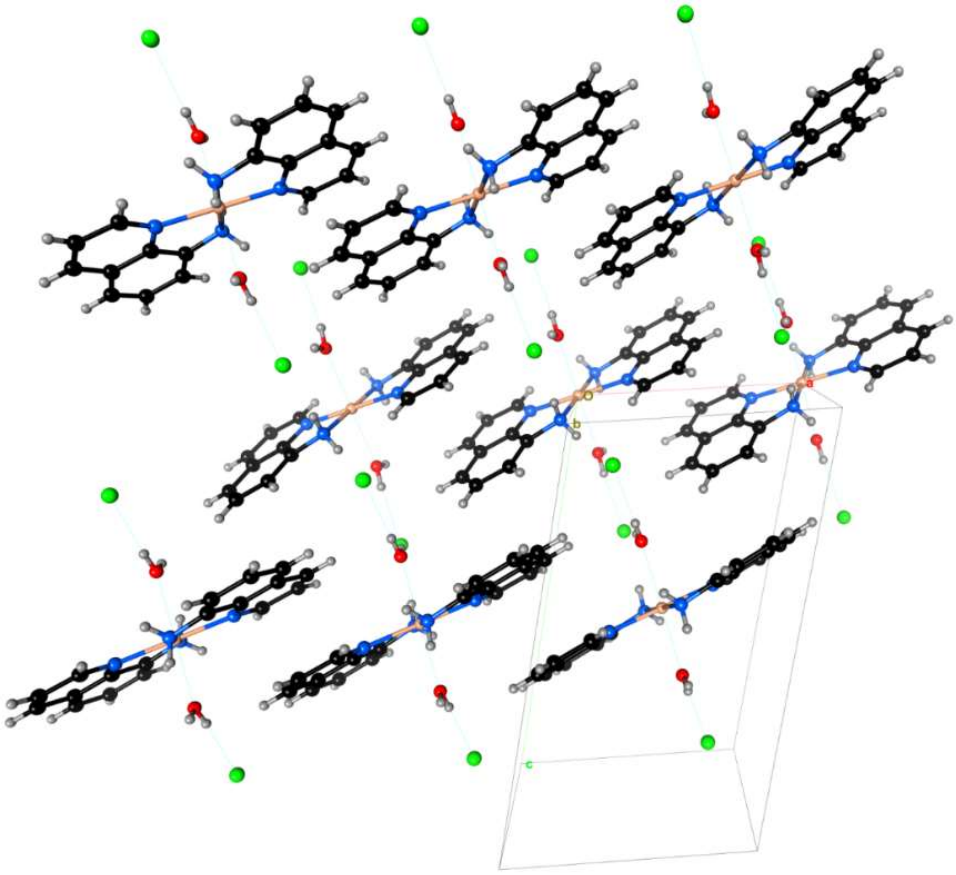

Fig. 5. Crystallographic autostereogram of the crystal packing along the *b* axis. OH···Cl^- hydrogen bonds and O···Cu coordination bonds are shown as dotted lines.

Table 2. Selected bond lengths (Å) and angles (º) for **(1)**.

Bond lengths (Å)			
Cu1-N2^{i}	2.007 (2)	C1-C2	1.408 (3)
Cu1-N2	2.007 (2)	C2-C3	1.369 (4)
Cu1-N1^{i}	2.023 (2)	C3-C4	1.407 (4)
Cu1-N1	2.023 (2)	C4-C5	1.416 (3)
Cu1-O1W^{i}	2.431 (2)	C4-C9	1.420 (3)
Cu1-O1W	2.431 (2)	C5-C6	1.359 (4)
N1-C1	1.315 (3)	C6-C7	1.407 (4)
N1-C9	1.365 (3)	C7-C8	1.361 (3)
N2-C8	1.448 (3)	C8-C9	1.414 (3)
Bond Angles (º)			
N2^{i}-Cu1-N2	180.0	N1-C1-C2	123.2 (2)
N2^{i}-Cu1-N1^{i}	83.44 (8)	C3-C2-C1	119.3 (2)
N2-Cu1-N1^{i}	96.56 (8)	C2-C3-C4	119.3 (2)
N2^{i}-Cu1-N1	96.56 (8)	C3-C4-C5	124.3 (2)
N2-Cu1-N1	83.44 (8)	C3-C4-C9	117.6 (2)
N1^{i}-Cu1-N1	180.0	C5-C4-C9	118.1 (2)
N2^{i}-Cu1-O1W^{i}	88.50 (7)	C6-C5-C4	120.8 (2)
N2-Cu1-O1W^{i}	91.50 (7)	C5-C6-C7	120.7 (2)
N1^{i}-Cu1-O1W^{i}	84.19 (7)	C8-C7-C6	120.4 (2)
N1-Cu1-O1Wi	95.81 (7)	C7-C8-C9	120.1 (2)
N2^{i}-Cu1-O1W	91.50 (7)	C7-C8-N2	124.3 (2)
N2-Cu1-O1W	88.50 (7)	C9-C8-N2	115.7 (2)
N1^{i}-Cu1-O1W	95.81 (7)	N1-C9-C8	117.9 (2)
N1-Cu1-O1W	84.19 (7)	N1-C9-C4	122.2 (2)
O1Wi-Cu1-O1W	180.0	C8-C9-C4	119.9 (2)
C1-N1-C9	118.4 (2)	C9-N1-Cu1	111.55 (16)
C1-N1-Cu1	129.74 (18)	C8-N2-Cu1	109.89 (15)
		Symmetry code : *(i)*	-*x*+1, -*y*+1, -*z*+1.

Table 3. Hydrogen bond and short inter-ion contact geometry in **(1)**.

D*–H···*A	***D*-H**	***H···A***	***D···A***	***D*-H···*A***
O1W-H11···Cl1	0.83	2.32	3.136 (2)	166
O1W-H12···Cl1^{ii}	0.83	2.33	3.151 (2)	165
N2-H22···Cl1^{ii}	0.88	2.49	3.294 (2)	154
N2-H21···Cl1^{iii}	0.89	2.36	3.245 (2)	174

Symmetry codes : (ii) $-x+{}^{3}/_{2}, y-½, -z+{}^{3}/_{2}$; (iii) $x-½, -y+½, z-½$; (iv) x-½, ${}^{3}/_{2}$-y, z -½

Table 4. Bond Distances (Å) Comparison in Cu(8-aq) isomer Complexes.

Complexes	**Cu-N$_{ring}$ (Exp)**	**Cu-N$_{amino}$**	**References**
[Cu(H$_2$O)$_2$(C$_9$H$_8$N$_2$)$_2$]. 2Cl$^-$	2.023 (2)	2.007 (2)	This work
[Cu(C$_9$H$_8$N$_2$)$_2$(Cl)(H$_2$O)]$^+$. Cl$^-$. H$_2$O	1.991 (10)- 2.033 (10)	1.985 (9)- 2.014 (10)	[46]
[Cu(8-aq)$_2$(NO$_3$)(H$_2$O)]. NO$_3$	2.023 (6)- 2.027 (6)	1.998 (6)- 2.007 (6)	[47]

4.2. Interactions and Hirshfeld surface analysis

It is critical to identify how atoms on the Hirshfeld Surface (HS) interact with atoms on neighboring molecules because this provides information about the packing of molecules [48-53]. When compared to other atoms present inside the HS, the H atoms located inside the HS interact the most with the atoms of molecules located outside the HS. The percentage contribution of H-ALL interaction is 41.8%, where ALL stands for all atoms of molecules located in the vicinity of HS (Table 5). The other major interactions are C-ALL (25.0%), Cl-ALL (16.3%), Cu-ALL (6.4%), N-ALL (4.7%) and C-ALL (3.8). The interaction of an atom in the vicinity of the HS with all of the atoms of the molecule existing inside the HS is also computed (Table 5). ALL-H interaction is also the main interaction at 37.8% and the percentage contributions of interactions are ALL-C (21.9%), ALL-Cl (18.8%), ALL-Cu (13.6%), ALL-N (4.7%) and ALL-O (3.4%).

The most abundant contacts are constituted by the O/N···HCl$^-$ strong hydrogen bonds followed by the weaker C···H-C and C-H···Cl$^-$ weak hydrogen bonds (Table 3). All the favorable interactions are over-represented, notably the strong H-bonds (E=3.5). The chloride anion is surrounded by hydrogen

atoms from the organic and water molecules. The copper cation has no contact with the chloride anion but is instead coordinated by the water oxygen and two nitrogen atoms and these contacts are the most enriched at high ratios E>5.7. In a crystal structure [46]of 8-aminoquinoline $CuCl_2$, devoid of water, the copper (II) cation is conversely coordinated by two nitrogen atoms and two chloride anions [54].

The C···C contacts are the third abundant type (Figure 6) and are remarkably enriched (E=2.57) due to extensive aromatic stacking between the 8-aminoquinoline molecules. The planar aromatic moieties show two orientations (forming an angle of 37.0°) in the crystal packing (Figure 5). The self-contacts are absent or strongly under-represented, except for the C···C type.

The Hirshfeld surface appears to have an equal share of hydrophobic (Hc and C) and hydrophilic (more charged) atoms. The crystal is constituted by an alternance of hydrophobic and hydrophilic layers parallel to the (b, a+c) plane (Figure 6). This can be seen in the contact statistics as both hydrophobic and hydrophilic contacts are enriched at E≅1.35. On the other hand, the cross contacts are disfavored at E=0.65 and consist mostly of weak C-H···Cl^- hydrogen bonds. The fingerprint plots (Figure 7) show two spikes at a short distance, constituted by the N···Cu coordination and the N-H···Cl strong hydrogen bonds.

The response of a crystal to an applied stress or force depends on the voids in the crystal packing. When voids are small, the atoms are strongly packed with each other, and the crystal can bear stress of a significant amount. The void was computed by using CrystalExplorer17 software (Figure 8). The void volume and surface area were found to be 73.48 $Å^3$ and 276.3 $Å^2$, respectively. The voids occupy only 7.8 % of the space in the crystal packing, indicating that the molecules are strongly held together through non-covalent interactions [55].

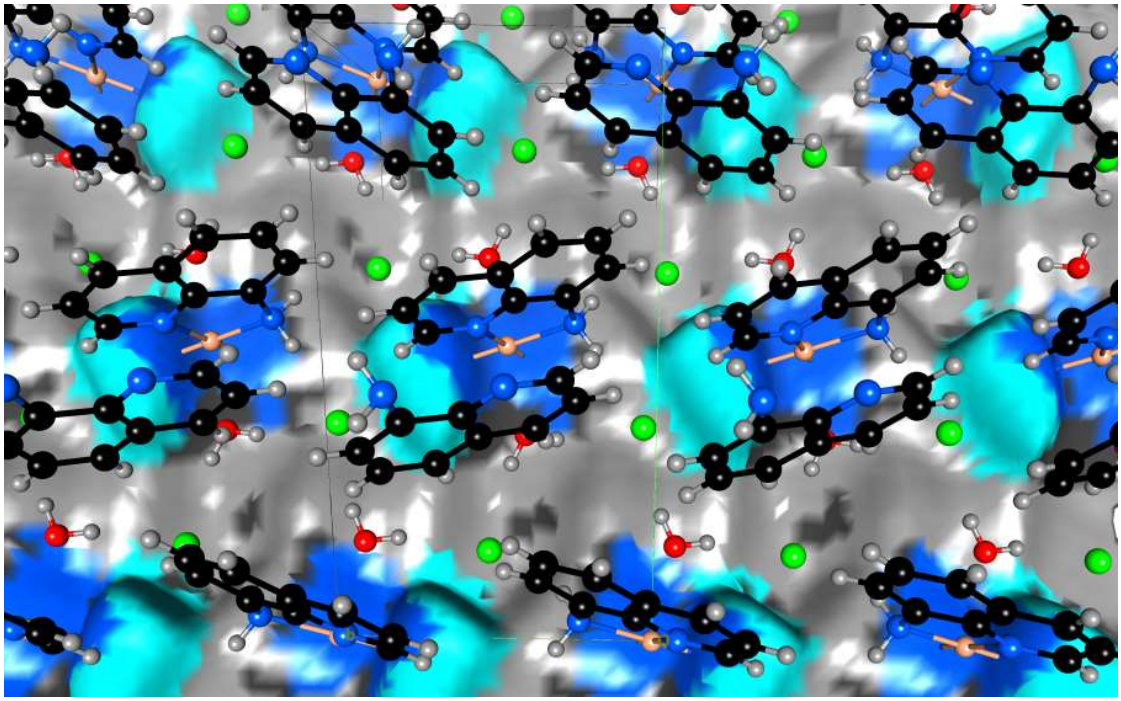

Fig. 6. Autostereogram of the Hirshfeld surface over an organic layer parallel to the (***b***, ***a***+***c***) plane. The unit cell is shown, and the ***b*** axis is horizontal, the ***c*** axis vertical. Surface color: grey: Hc, blue: nitrogen; light blue: Hn, dark grey: carbon. Oxygen and chlorine atoms are in red and green, respectively.

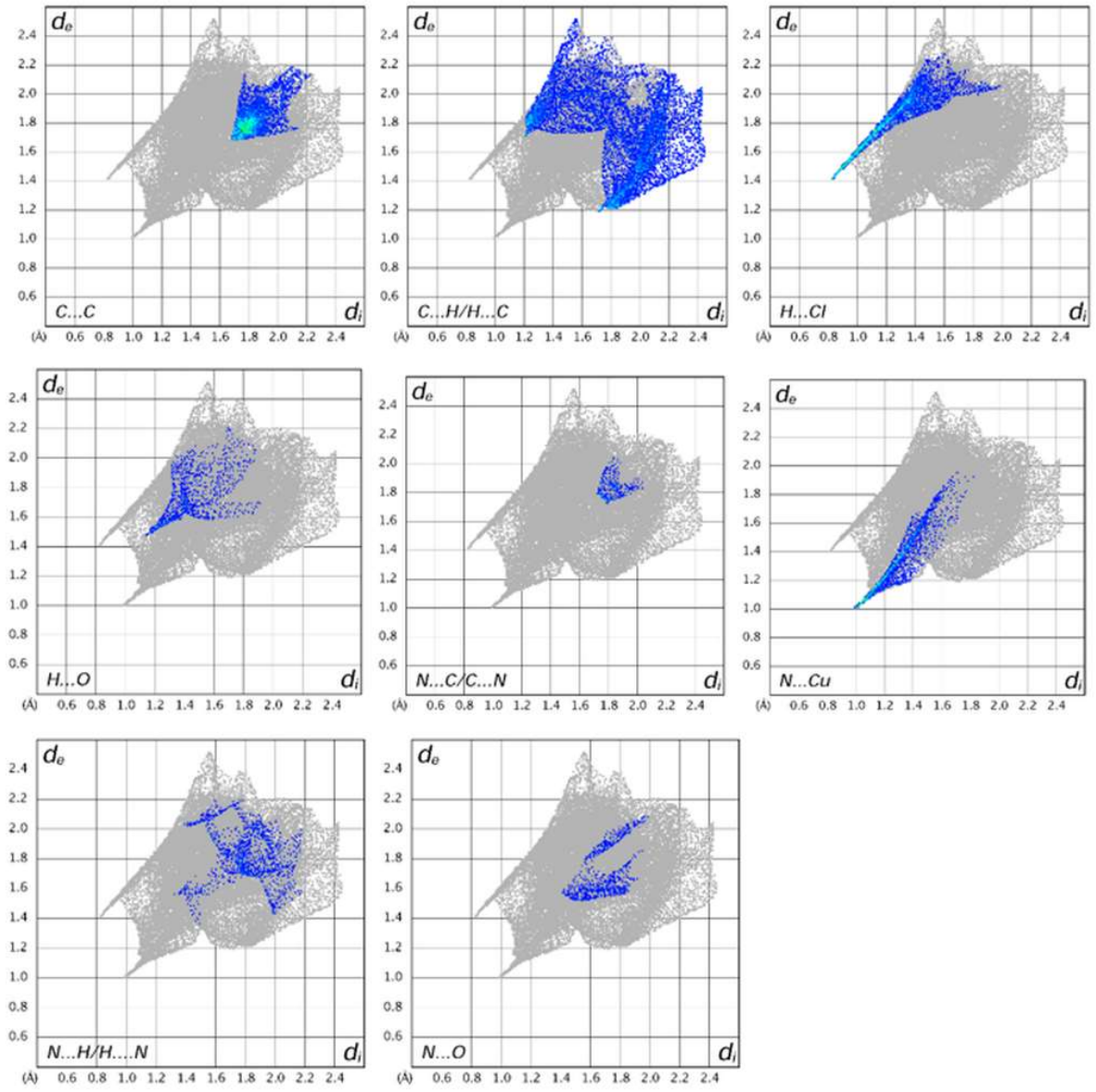

Fig. 7. Fingerprint plot of the main interactions around the 8-aminoquinoline ligand.

Table 5. Analysis of contacts on the Hirshfeld surface. Reciprocal contacts X···Y and Y···X are merged. The second line shows the chemical content on the surface. The % of contact types between chemical species is given followed by their enrichment ratio. The major contacts as well as the major enriched ones are highlighted in bold characters. The hydrophobic hydrogen atoms bound to carbon (Hc) were distinguished from the more polar ones bound to oxygen or nitrogen (Ho/n). In the last 3 lines, the contacts have been regrouped in terms of hydrophobic atoms (C and Hc) and hydrophilic (the others).

atom	**Ho/n**	**C**	**N**	**O**	**Cl**	**Cu**	**Hc**
surface %	**16.6**	**24.1**	**5.7**	**4.8**	**16.1**	**6.3**	**26.3**
Ho/n	1.1						
C	0.8	**13.8**			% contacts		
N	0.0	0.5	0.0				
O	0.1	0.5	0.3	0.0			
Cl	**19.9**	1.5	0.0	0.0	0.0		
Cu	1.3	0.9	**7.2**	3.7	0.0	0.0	
Hc	**8.8**	**16.7**	0.4	2.6	**15.9**	0.4	3.5
Ho/n	0.41						
C	0.11	**2.57**			Rxy		
N	0	0.15	0				
O	0.04	0.21	0.39	0			
Cl	**3.5**	0.19	0	0	0		
Cu	0.64	0.3	**7.8**	**5.7**	0	0	
Hc	1.11	**1.47**	0.11	1.04	**1.83**	0.13	0.59
% surface	hydro-	50.5	Hydro-	49.5			
% contacts	phobic	34.0	philic	33.6	Cross	32.4	
enrichment		1.34		1.37		0.65	

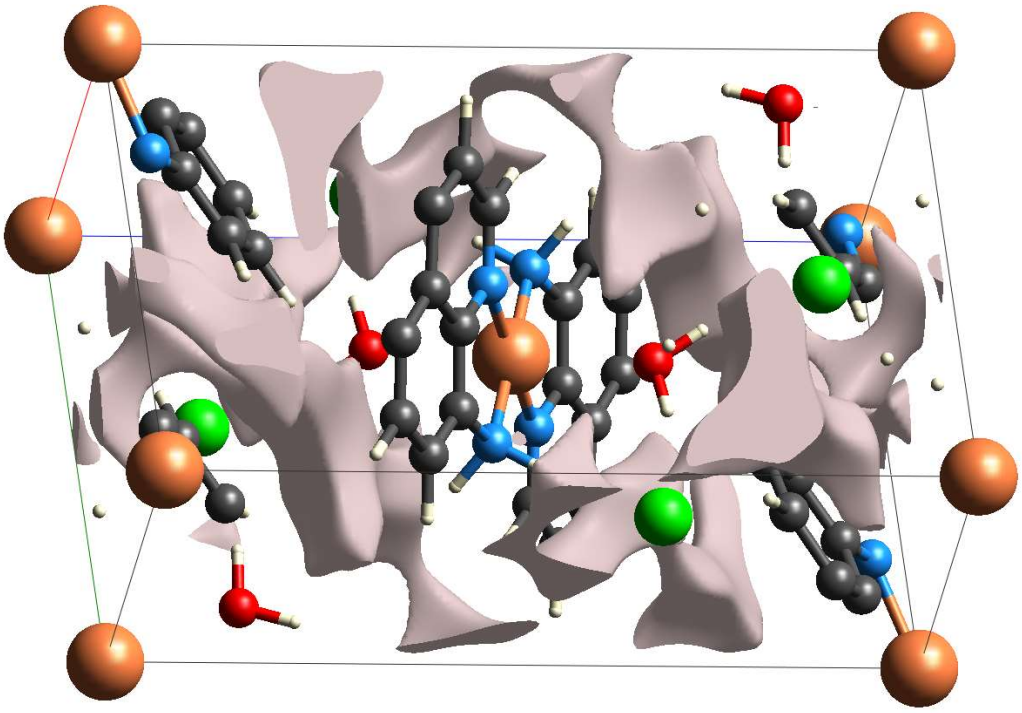

Fig. 8. Void analysis in the crystal packing of the title complex at 0.002 a.u. electron density (**c** horizontal, **b** vertical).

4.3. Molecular descriptors and Fukui indices

4.3.1. Calculated descriptors

The Frontier Molecular Orbitals (HOMO and LUMO) and their energies are very useful for chemists, and they are very important in quantum chemistry. They are used to determine the most reactive position in electronic systems and explain several types of reaction in a conjugate system [56].

It is well known that the conjugated molecules are characterized by a small energy that separates the orbitals (HOMO-LUMO), which is the result of a significant degree of intramolecular charge transfer from the end-capping electron-donor groups to the acceptor groups by the conjugate route [57]. Therefore, the highest occupied molecular orbital (HOMO) and the lowest unoccupied molecular orbital (LUMO) are the main orbitals involved in chemical stability [58]. Thus, the energy gap gives an idea of the stability of the molecule. The HOMO represents the ability to donate an electron. However, the LUMO represents the ability to obtain an electron. The optimized structure of complex (**1)** and the HOMO and LUMO energies are shown in Figure 9. The optimized structural parameters, bond lengths and bond angles, are presented in Table 1S.

The HOMO is located on the Cu, Cl and N atoms (Figure 8b and e), while the LUMO is located on the quinolone rings except nitrogen atoms (Figure 9c and f). The HOMO → LUMO transition involves an electron density transfer to the cyclic group from the CuN_4O_2 group. Fig.9g shows the density of states and the energy gap of complex **(1)**. The intensity of the HOMO is very high, and this is due to the presence of the copper element.

$$E_{HOMO} = -4.95 eV$$

$$E_{LUMO} = -3.22 eV$$

$$\Delta E = E_{LUMO} - E_{HOMO} = 1.73 eV$$

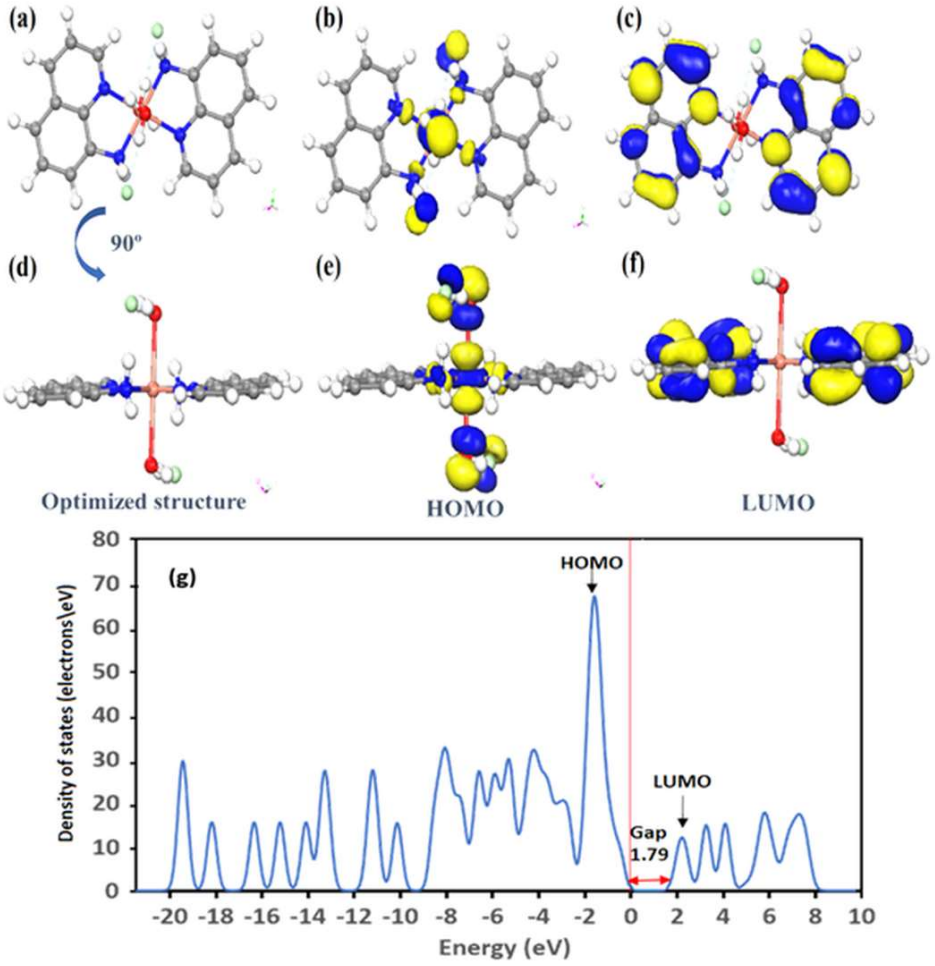

Fig. 9. Optimized structure **(a)**, and Frontier molecular orbitals **[(b, e) HOMO, (c, f) LUMO** and **(g)** the density of states of **(1)**.

HOMO energy is directly related to ionization potential (IP), whereas LUMO energy is directly related to electron affinity (EA) [59]:

$$IP = -E_{HOMO} = 4.95 \text{ eV}. \quad (1)$$

$$EA = -E_{LUMO} = 3.22 \text{ eV} \quad (2)$$

The Mulliken electronegativity (χ) and the Absolute hardness (η) can also deduced from the value of E_{HOMO} and E_{LUMO} as follow [60,61]:

$$\chi = \frac{IP + EA}{2}, \quad \chi = -\frac{E_{LUMO} + E_{HOMO}}{2} = 4.09 \text{ eV} \quad (3)$$

$$\eta = \frac{IP - EA}{2}, \quad \eta = -\frac{E_{LUMO} - E_{HOMO}}{2} = 0.86 \text{ eV} \quad (4)$$

4.3.2. Fukui function

Fukui function is one of the most important factors for the determination of the chemical reactivity and the electrophilic and nucleophilic sites [56, 62]. The Fukui indices as a function of the atomic charges are given by:

$$f_k^- = q_k(N) - (N\text{-}1) \text{ (for electrophilic attack)} \quad (5)$$

$$f_k^+ = q_k(N\text{+}1) - (N) \text{ (for nucleophilic attack)} \quad (6)$$

$$f_k^0 = [q_k(N\text{+}1) - q_k(N\text{-}1)]/2 \text{ (for radical attack)} \quad (7)$$

Where q_k is the electronic charge of atom k and N is the number of electrons. The values of the condensed Fukui function (f_k^-, f_k^+ , f_k^0), were calculated for electrophilic, nucleophilic, and radical attacks have been performed using the Dmol^3 code. The results are summarized in Table 6.

Table 6 shows that the copper cation has the highest value of f_k^+. Thus, this atom is the most favorite site for electrophilic attack. However, nitrogen N2 presents the most favorite site for the nucleophile attack as it has the highest f_k^- value. Using the same reasoning, a radicular attack is very favorable on copper. The results obtained from the Fukui function and from the analysis of the LUMO and HOMO orbitals are in good agreement. The two methods lead to the same predictions of the sites that are most electron deficient.

Table 6. Fukui Indices for Radical Attack f_k^0, Nucleophilic Attack f_k^+ and for Electrophilic Attack f_k^-.

atom	f_k^0		f_k^+		f_k^-	
	Mulliken	Hirshfeld	Mulliken	Hirshfeld	Mulliken	Hirshfeld
Cu(1)	0.081	0.118	**0.117**	0.161	0.046	0.075
Cl(1)	0.042	0.042	0.030	0.03	0.054	0.054
Ow	0.003	0.01	0.003	0.01	0.004	0.01
Hw	0.006	0.005	0.006	0.004	0.006	0.006
Hw	0.014	0.01	0.016	0.011	0.013	0.009
N1	0.001	0.027	-0.006	0.022	0.008	0.032
N2	0.053	0.058	0.046	0.052	**0.059**	0.064
H	0.039	0.029	0.040	0.029	0.038	0.029
H	0.013	0.013	0.013	0.012	0.012	0.014
C1	0.026	0.023	0.028	0.023	0.024	0.023
H	0.027	0.016	0.028	0.016	0.026	0.016
C2	0.014	0.021	0.013	0.022	0.014	0.02
H	0.021	0.015	0.022	0.015	0.021	0.015
C3	0.026	0.026	0.027	0.027	0.025	0.025
H	0.019	0.014	0.020	0.014	0.019	0.014
C4	0.009	0.015	0.009	0.015	0.009	0.015
C5	0.020	0.022	0.020	0.022	0.021	0.022
H	0.019	0.013	0.018	0.013	0.019	0.013
C6	0.012	0.019	0.012	0.019	0.012	0.019
H	0.017	0.012	0.017	0.012	0.017	0.012
C7	0.022	0.023	0.022	0.023	0.023	0.023
H	0.021	0.014	0.021	0.014	0.021	0.014
C8	0.002	0.004	0.002	0.003	0.001	0.005
C9	0.032	0.012	0.034	0.011	0.030	0.013

4. Conclusion

In summary, we have synthesized and structurally characterized a new copper (II) isomer $[Cu(H_2O)_2(C_9H_8N_2)_2]Cl_2$. The X-ray diffraction analysis shows that the crystal packing is stabilized by two O-H···Cl^-, two N-H···Cl^- and five C-H···Cl^- (up to d_{HCl} = 3.36Å) hydrogen bonds as well as aromatic stacking interactions. The Hirshfeld surface analysis shows that the Cu(II)···N, Cu(II)···O, Ho/n···Cl^-, C···C, Hc···Cl^- and C···Hc are the most over-represented contacts, by decreasing order. The PBE functional method with a DNP basis set is used to calculate Fukui indices, which are used to model chemical reactivity and site selectivity (1). The most important site for the nucleophilic attack of **(1)** is the nitrogen atom of the quinolone rings, whereas the preferred site for the electrophilic attack is the copper atom. The HOMO-LUMO energy gap and the different chemical reactivity descriptors show the intramolecular charge transfer taking place within the molecule and the significant antioxidant ability of **(1)**.

Availability of data and materials Experimental X-ray diffraction data are available from the Cambridge Crystallographic Data Centre on request quoting the deposition numbers CCDC 2054557.

Authors contributions

All authors, Z. Setifi, H. Ferjani, Y. Ben Smida, C. Jelsch, F. Setifi, C. Glidewell, made contributions to this study.

Funding The authors thank the Algerian ministère de l'Enseignement Supérieur et de la Recherche Scientifique (MESRS), the Direction Générale de la Recherche Scientifique et du Développement Technologique (DGRSDT) as well as the Université Ferhat Abbas Sétif 1 for Financial support.

Competing Interests: the authors declare no competing interests.

References

[1] Setifi Z, Lehchili F, Setifi F, Beghidja A, Ng S.W, Glidewell C (2014) Acta Crystallogr. C Struct. Chem. 70:338-341.

[2] Benamara N, Setifi Z, Yang C.-I, Bernès S, Geiger D.K, Kürkçüoğlu G.S, Setifi F, Reedijk J (2021) Magnetochemistry 7(4):50.

[3] Dmitrienko A.O, Buzin M.I, Setifi Z, Setifi F, Alexandrov E.V, Voronova E.D, Vologzhanina A.V, Dalton Trans (2020) 49(21):7084-7092.

[4] Setifi F, Konieczny P, Glidewell C, Arefian M, Pelka R, Setifi Z, Mirzaei M (2017) J. Mol. Struct. 1149:149-154.

[5] Setifi Z, Ghazzali M, Glidewell C, Perez O, Setifi F, Gómez-García C.J, Reedijk J, Polyhedron (2016) 117:244-248.

[6] Pramanik S, Pathak S, Frontera A, Mukhopadhyay S (2022) J. Mol. Struct. 1265:133358.

[7] Das A, Sharma P, Gomila R.M, Frontera A, Verma A.K, Sarma B, Bhattacharyya M.K (2022) Polyhedron 213:115632.

[8] Gomila R.M, Bauza A, Mooibroek T.J and Frontera A (2021) Dalton Trans 50:7545-7553.

[9] Mautner F.A, Bierbaumer F, Fischer R.C, Vicente R, Tubau À, Ferran A, Massoud S.S, Crystals (2021)11:179.

[10] Nehra P, Khungar B, Singh R.P, Sivasubramanian S.C, Jha P.N, Saini V (2018) Inorganica Chim Acta. 478:260-267

[11] Benmansour S, Setifi F, Triki S, Gomez-Garcia C.J (2012) Inorg Chem 51(4):2359-2365.

[12] Benmansour S, Setifi F, Gómez-García C.J, Triki S. Coronado E (2008) Inorganica Chim Acta 361(14-15):3856-3862.

[13] Atmani C, Setifi F, Benmansour S, Triki S, Marchivie M, Salaün J.-Y, Gómez-García C.J (2008) Inorg Chem Commun 11(8):921-924.

[14] Yan L, Wang X, Wang Y, Zhang Y, Li Y, Guo Z (2012) J Inorg Biochem 106(1):46-51.

[15] Zelenka K, Brandl H, Spingler B, Zelder F (2011) Dalton Trans 40(38):9665-9667.

[16] Wang K, Shen M, Sun W.-H (2009) Dalton Trans 21:4085-4095.

[17] Setifi F, Milin E, Charles C, Thétiot F, Triki S, Gomez-Garcia C.J (2014) Inorg Chem 53(1):97-104.

[18] Genre C, Jeanneau E, Bousseksou A, Luneau D, Borshch S.A, Matouzenko G.S (2008) Chem Eur J 14(2), 697-705.

[19] Genre C, Matouzenko G.S, Jeanneau E, Luneau D (2006) New J Chem 30(11):1669-1674.

[20] Boonkitpatarakul K, Smata A, Kongnukool K, Srisurichan S, Chainok K, Sukwattanasinitt M (2018) J Lumin 198:59-67.

[21] Morales L, Toral M.I, Álvarez M.J (2007) Talanta 74(1):110-118.

[22] Bortoluzzi M, Paolucci G, Pitteri B, Vavasori A (2006) Inorg Chem Commun 9(12):1301-1303.

[23] Rahmati Z, Mirzaei M, Chahkandi M, Mague J.T (2018) Inorganica Chim Acta 473:152-159.

[24] Paira M, Dinda J, Lu T.-H, Paital A, Sinha C (2007) Polyhedron 26(15):4131-4140.

[25] Massoud S.S, Louka F.R, Mikuriya M, Ishida H, Mautner F.A (2009) Inorg Chem Commun 12(5):420-425.

[26] Mautner F.A, Jantscher P.V, Fischer R.C, Reichmann K, Massoud S.S, Speed S, Vicente R (2021) Polyhedron 204:115263.

[27] Mautner F.A, Jantscher P.V, Fischer R.C, Torvisco A, Reichmann K, Salem N.M.H, Gordon K.J, Louka F.R, Massoud S.S (2021) Crystals 11(2):181.

[28] Palion-Gazda J, Choroba K, Machura B, Świtlicka A, Kruszyński R, Cano J, Lloret F, Julve M (2019) Dalton Trans 48:17266-17280.

[29] Boča R, Boča M, Gembický M, Jäger L, Wagner C, Fuess H (2004) Polyhedron 23(15):2337-2348.

[30] Mautner F.A, Traber M, Fischer R.C, Massoud S.S, Vicente R (2017) Polyhedron 138:13-20.

[31] Setifi Z, Geiger D, Jelsch C, Maris T, Glidewell C, Mirzaei M, Arefian M, Setifi F (2018) J Mol Struct 1173:697-706.

[32] Setifi Z, Bernès S, Pérez O, Setifi F, Rouag D.A (2015) Acta Cryst E71:698-701.

[33] Setifi Z, Setifi F, Saadi M, Rouag D.A, Glidewell C (2014) Acta Crys C70:359-363.

[34] Setifi Z, Zambon D, Setifi F, El-Ghozzi M, Mahiou R, Glidewell C (2017) Acta Cryst C73:674-681.

[35] CrysAlis, P., Agilent technologies. Yarnton, Oxfordshire, England, 2011.

[36] Sheldrick G.M (2015) Acta Cryst A 71(1):3-8.

[37] Brandenburg K, Putz H, Diamond. Crystal Impact GbR, Bonn, Germany, (2006).

[38] Guillot B, Enrique E, Huder L, Jelsch C (2014) Acta Cryst 70:C279.

[39] Delley B (2000) J Chem Phys 113(18):7756-7764.

[40] Mulliken R (1955) J Chem Phys 23(10):1841-1846.

[41] Delley B (2006) J Phys Chem A 110(50):13632-13639.

[42] Xu H, Guo C (2012) Acta cryst E 68(1):m3-m3.

[43] Kawamoto K, Shibahara T (2012) Acta cryst E 68(2):m208-m208.

[44] Li Z, Wang S, Zhang Q, Yu X (2007) Acta cryst E 63(11):m2781-m2781.

[45] Kovbasyuk L.A, Babich O.A, Kokozay V.N (1997) Polyhedron 16(1):161-163.

[46] Zhang G, Zhang Y.Z, Lo W.-F, Jiang J, Golen J.A, Rheingold A.L (2016) Polyhedron 103:227-234.

[47] Mirzaei M, Eshtiagh-Hosseini H, Bolouri Z, Rahmati Z, Esmaeilzadeh A, Hassanpoor A, Bauza A, Ballester P, Barceló-Oliver M, Mague J.T, Notash B, Frontera A (2015) Cryst Growth Des 15(3):1351-1361.

[48] Setifi Z, Ferjani H, Jelsch C, Glidewell C, Dege N, Setifi F (2021) J Inorg Organomet Polym Mater 31:3054-3061.

[49] Shaaban S, Ferjani H, Yousef T & Abdel-Motaal M (2022) J Inorg Organomet Polym Mater 32:1878-1890.

[50] Azam M, Al-Resayes S, Trzesowska-Kruszynska A, Kruszynski R (2022) J Mol Struct 1259:132727.

[51] Azam M, Sahoo P.K, Ranjan Mohapatra K, Kumar M, Ansari A, Moon S, Chutia A, Al-Resayes S, Biswal S.K (2022) J Mol Struct 1251:132039.

[52] Kansız S, Tolan A, Azam M, Dege N, Alam M, Sert Y, I.Al-Resayes S, İçbudak H (2022) Polyhedron 218:115762

[53] Azam M, Velmurugan G, Trzesowska-Kruszynska A, I.Al-Resayes S, Kruszynski R, Venuvanalingam P (2022) 534:120807

[54] Mao R, Frey A, Balon J, Hu X (2018) Nat Catal 1(2):120-126.

[55] Turner M.J, McKinnon J.J, Jayatilaka D, Spackman M.A (2011) Cryst Eng Comm13(6):1804-1813.

[56] Fukui K, Yonezawa T, Shingu H (1952) J Chem Phys 20(4):722-725.

[57] Choi C.H, Kertesz M (1997) J Phys Chem A 101(20):3823-3831.

[58] Gunasekaran S, Balaji R.A, Kumeresan S, Anand G, Srinivasan S (2008) Can J Anal Sci Spectrosc 53(4):149-162.

[59] Gholami M, Danaee I, Maddahy M.H, RashvandAvei M (2013) Ind Eng Chem Res 52(42):14875-14889.

[60] Sastri V, Perumareddi J (1997) Corros Sci 53(08):617-622.

[61] Pearson R.G (1988) Inorg Chem 27(4):734-740.

[62] Lgaz H, Salghi R, Ali I.H (2018) Int J Electrochem Sci 13:250-264.